

To appear in Ap J.

Extended ionized gas emission and kinematics of the compact group galaxies in HCG 16: Signatures of mergers

C. Mendes de Oliveira¹

Instituto Astronômico e Geofísico (IAG), Av Miguel Stefano 4200, 04301-904, São Paulo, Brazil

H. Plana² and P. Amram

Observatoire de Marseille, 2 Place Le Verrier, 13248 Marseille, Cedex 04, France

M. Bolte

Lick Observatory, Board of Studies in Astronomy and Astrophysics, University of California,
Santa Cruz, California 95064

and

J. Boulesteix

Observatoire de Marseille, 2 Place Le Verrier, 13248 Marseille, Cedex 04, France

ABSTRACT

We report on kinematic observations of $H\alpha$ emission from four late-type galaxies of the Hickson Compact Group 16 (H16 a,b,c and d) obtained with a scanning Fabry-Perot interferometer and samplings of 16 km s^{-1} and $1''$. The velocity fields show kinematic peculiarities for three of the four galaxies: H16b, c and d. Misalignments between the kinematic and photometric axes of gas and stellar components (H16b,c,d), double gas systems (H16c) and severe warping of the kinematic major axis (H16b and c) were some of the peculiarities detected.

We conclude that major merger events have taken place in at least two of the galaxies of the group, H16c and d, based on their significant kinematic peculiarities, their double nuclei and high infrared luminosities. Their $H\alpha$ gas content is strongly spatially concentrated – H16d contains a peculiar bar-like structure confined to the inner $\sim 1 \text{ h}^{-1} \text{ kpc}$ region. These observations are in agreement with predictions of simulations, namely that the gas flows towards the galaxy nucleus during mergers, forms bars and fuels the central activity. Galaxy H16b, an Sb galaxy, also presents

¹present address: Universitäts-Sternwarte, Ludwig-Maximilians-Universität, Scheinersstrasse 1, 81679 Muenchen, Germany

²present address: Instituto Astronômico e Geofísico (IAG), Av Miguel Stefano 4200, CEP: 04301-904, São Paulo, Brazil

some of the kinematic evidences for past accretion events. Its gas content, however, is very sparse, limiting our ability to find other kinematic merging indicators, if they are present. We find that the merger remnants in the compact group HCG 16 have significantly *smoother* optical profiles than isolated mergers, i.e., they show an amorphous morphology and no signs of tidal tails. Tidal arms and tails formed during the mergers may have been stripped by the group potential (Barnes & Hernquist 1992) or alternatively they may have never been formed.

The velocity field of the galaxy H16a shows grand-design isovelocity lines with no signs of disturbances inside a radius of $\sim R_{25}$. This result is contrary to expectations given that the galaxy has a high infrared luminosity, central activity, tidal tails at large radii and it is embedded in a common group envelope observed in HI and x-rays. The normality of the velocity field suggests that this galaxy may be a fairly recent acquisition of the group.

Our observations suggest that HCG 16 may be a young compact group in formation through the merging of close-by objects in a dense environment.

Subject headings: Interferometry: Fabry-Perot – Galaxies: Irregular and spiral – Galaxies: ISM – Galaxies: kinematics, dynamics and interaction – Galaxies: photometry – Galaxies: individual HCG 16a or NGC 835, HCG 16b or NGC 833, HCG 16c or NGC 838, HCG 16d or NGC 839.

1. Introduction

Nearby compact groups may provide one of the best laboratories for studying the effects of on-going collisions on the structure and dynamics of galaxies. One of the most dense compact groups known is HCG 16 (H16), or Arp 318, originally catalogued by Hickson (1982) as an association of four late-type galaxies at $V \sim 4000 \text{ km s}^{-1}$ with a small velocity dispersion of 123 km s^{-1} and a median galaxy-galaxy projected separation of $44 \text{ h}^{-1} \text{ kpc}$ (Hickson et al. 1992, h is the dimensionless Hubble constant $H_o/100 \text{ km sec}^{-1} \text{ Mpc}^{-1}$). Ribeiro et al. (1996) found three other bright galaxies near the group, in the same redshift range, within a median radius of $0.197 \text{ h}^{-1} \text{ Mpc}$. All seven galaxies were found to have nuclear emission lines, making H16 the highest concentration of starburst and active nuclei galaxies in the nearby universe.

ROSAT observations of the group (Ponman et al. 1996) revealed an intragroup medium with a total extent of $\sim 400 \text{ h}^{-1} \text{ kpc}$, a temperature of 0.3 KeV and density of $N_H = 2.05 \times 10^{20} \text{ cm}^{-1}$. Such density and temperature are typical of compact groups of galaxies, which were shown to fit well on the extension of the correlations between the X-ray luminosity and both the gas temperature and velocity dispersion of clusters of galaxies (although with a steeper slope than for clusters (Ponman et al. 1996)). The presence of diffuse X-ray emission around H16 is a strong evidence that this is a genuine group.

Compact groups that are true high-density systems, as H16 seems to be, provide excellent environments in which to study the properties of merger galaxies. Such a study for a compact group galaxy is important not only to investigate the process of galaxy formation through mergers but it may also provide important information on the dynamical evolutionary stage of the compact group.

In this paper we investigate the dynamical state of the Hickson compact group 16 through the study of the detailed 2-D kinematics of four of its member galaxies: H16a (NGC 835, Mrk 1022), H16b (NGC 833), H16c (NGC 838, Mrk 1021) and H16d (NGC 839). The four galaxies are optically luminous systems, with M_B ranging from $-20.3 + 5 \log h$ to $-19.5 + 5 \log h$. H16a, c and d are strong radio and infrared sources (Allam et al. 1996, Menon 1995). Boselli et al. (1996) report on CO observations for three of the four galaxies and calculate large masses of molecular gas. Analysis of their central spectra shows that H16a and d are LINERs, H16b is a Seyfert galaxy and H16c has a starburst nucleus (Coziol et al. 1998). Rubin, Hunter & Ford (1991, RHF91) obtained rotation curves (RCs) for the four galaxies and found they have “abnormal” shapes, a common feature among strongly interacting and merging galaxies.

H α emission-line observations of H16 a,b,c,d obtained with a scanning Fabry-Perot are used here to derive the spatial distribution and kinematics of their warm gas content. The warm gas is a good tracer of the total gas mass (that is gas in all phases) in a galaxy (Schommer et al. 1993) and it should also be a good tracer of the potential of the galaxy. The details of the kinematics of the emission-line velocity field can be used as diagnostics of the gaseous merger dynamical state.

The organization of this article is as follows: Section 2 gives details of the observations and data reduction. In Section 3, we present the results for the photometry, the internal kinematics and the various mass determinations of the galaxies. Section 4 contains the discussion and our conclusions.

2. Observations

2.1. Photometric data

Images of H16a,b,c,d, in R and I were available for this study. The CCD R-band images were taken as part of a large study of the systematic properties of galaxies in compact groups. Details of these data are described in Hickson et al. (1989). The images have kindly been made available by P. Hickson. The I-band image was a 600s-frame (15' on a side, 0.44 arcsec pixels) taken with the 1.5m telescope at the Cerro Tololo Interamerican Observatory in October 1997. The mean seeing values for the R and I images were 1".5 and 1".2 respectively.

Luminosity, ellipticity and position angle (PA) profiles were determined for H16b, c and d, using the ISOPHOTE package in STSDAS (Jedrzejewski 1987). H16a is not well described by concentric elliptical isophotes and therefore no fit of this galaxy was attempted.

2.2. Fabry-Perot data

Observations were carried out with the Fabry-Perot instrument CIGALE mounted on the ESO 3.6m telescope in August 1995. CIGALE is composed of a focal reducer (bringing the original f/8 focal ratio of the Cassegrain focus to f/2), a scanning Fabry-Perot, a narrow band interference filter and an Image Photon Counting System detector (IPCS). The IPCS, with a time sampling of 1/50 s and zero readout noise makes it possible to scan the interferometer rapidly (typically 5 s per channel) avoiding sky transparency, airmass and seeing variation problems during the exposures.

Table 1 contains the journal of the observations. The exposure times were two hours for each of two pointings, one on H16ab and one on H16cd. The two observed fields are represented with boxes in Fig. 1. Table 2 presents general information on the four observed galaxies.

Reduction of the data cubes were performed using the CIGALE/ADHOC software (Boulesteix et al. 1993). The data reduction procedure has been extensively described in Amram et al. (1996) and references therein.

Wavelength calibrations were obtained by scanning the narrow Ne 6599 Å line under the same conditions as the observations. The relative velocities with respect to the systemic velocity are very accurate, with an error of a fraction of a channel width ($< 3 \text{ km s}^{-1}$) over the whole field.

The signal measured along the scanning sequence was separated into two parts: (1) an almost constant level produced by the continuum light in a 24 Å passband around H α (continuum map), and (2) a varying part produced by the H α line (monochromatic map). The continuum level was taken to be the mean of the three faintest channels, to avoid channel noise effects. The monochromatic map was obtained by integrating the monochromatic profile in each pixel. The velocity sampling was 16 km s^{-1} . The monochromatic maps had one-pixel resolution in the center of the galaxies. Spectral profiles were binned in the outer parts (to 5x5 pixels) in order to increase the signal-to-noise ratio. OH night sky lines passing through the filters were subtracted by determining the level of emission away from the galaxies (Laval et al. 1987).

A rough flux calibration of the monochromatic images was attempted by adjusting the flux levels to those of the calibrated image of the Cartwheel galaxy, obtained in the same run (see details of how the Cartwheel galaxy image was calibrated in Amram et al. 1998). H α profiles for the H16 galaxies were measured to a minimum flux density between $0.1 \times 10^{-17} \text{ erg s}^{-1} \text{ cm}^{-2} \text{ arcsec}^{-2}$ and $0.7 \times 10^{-17} \text{ erg s}^{-1} \text{ cm}^{-2} \text{ arcsec}^{-2}$ (corresponding to a S/N between three and eight).

3. Results

3.1. Morphology from the R, I and continuum images

Fig. 1 is the I-band image of the group with contours obtained from the continuum images superimposed.

3.1.1. *H16ab*

H16a and H16b are on the top right of Fig. 1 (H16a is the galaxy further to the east). They have been morphologically classified as early-type spiral galaxies (SBab and Sab respectively) by Hickson (1993) from inspection of CCD images. This classification is in general agreement with morphological classifications given by RHF91 and the RC3. The morphologies of H16a and H16b have been described in detail by RHF91. We confirm the central dust and the low-surface brightness tidal tails to the east (and a shorter one to the south) of H16a extending over 20 h^{-1} kpc. Hunsberger et al. (1996) detected three dwarf galaxy candidates on the eastern tail of H16a (discussed in Section 4.3). For H16b, the subtraction of a model galaxy with concentric elliptical isophotes uncovered an asymmetric cone-like structure to the west of the galaxy.

3.1.2. *H16c*

H16c and H16d, on the top and lower left of Fig. 1, have been classified as Irregular galaxies by Hickson (1993) and as S0 pec by de Vaucouleurs et al. (1991) (the RC3 catalog). The amorphous shapes of these galaxies make it difficult to visually determine if they are either bulge or disk dominated systems. R-band images of the central parts of these two galaxies are shown in Fig. 2.

H16c has two bright centers $\sim 2''$ apart (see Fig. 2a). The resolution of the Fabry-Perot image (Fig. 9a) is too low to separate the two nuclei. Neither of the two bright nuclei coincide with the center of the outer (outside of $10''$) isophotes of the galaxy. A bright extension of $\sim 5''$ directly west from both centers is also detected (see Fig. 2a). This extension is seen in the R, I, continuum and monochromatic images.

Fig. 3 presents the surface brightness profiles of H16c obtained by fitting the galaxy with concentric elliptical isophotes. Profiles are obtained from the emission-line image and continuum-image in order to check if reasonable fits can be found to exponential or de Vaucouleurs $r^{1/4}$ profiles. The data are plotted in linear scale (radius in arcsec) for the two curves to the left of the diagram and in radius to the power $1/4$, for the two curves to the right of the diagram. The profiles are not well fit by an $r^{1/4}$ or linear profile. It is evident, however, that the slope of the monochromatic profile (gaseous component) is steeper than the slope of the continuum image (stellar component) outside a radius of 5 arcsec. This is typical for gaseous disks in elliptical and lenticular galaxies.

A dust lane of ~ 30 -arcsec diameter crosses H16c from southeast to northwest, at PA $\sim 120^\circ$ (all PA measurements are made from north to east). The galaxy contains patchy dust throughout its center (within a radius of 10 – 15 arcsec). Outside this radius the subtraction of a concentric-elliptical isophote-model shows clean residuals. At large radii H16c has non-concentric isophotes, whose centers are displaced in the direction of H16d (Fig. 1).

3.1.3. H16d

Dust is also detected in H16d, inside the central 15-arcsec radius. In addition, H16d has a high surface brightness nucleus in the inner 2-arcsec radius (Fig. 2b). A “bar-like feature” is visible out to 5'' and is embedded in dust. These features are also present but seem to be less prominent in the I image. The effect of these features can be noted in the ellipticity, PA and $\cos(4\theta)$ R and I profiles shown in Fig. 4, for the inner region of the galaxy. The surface-brightness profiles in the R and I filters agree well except for the $\cos(4\theta)$ -diagram. Outside a radius of 8 arcsec the galaxy is very flat (ellipticity=0.55). The effect of the bright nucleus and of the central bar-like structure in the inner 2 and 5 arcsec respectively is to cause an increase in the galaxy ellipticity, a variation in the PA (with two discontinuities) and peaks in the $\cos(4\theta)$ profile. These peaks are much more prominent in the R than in the I-band images (seen also in the $\cos(4\theta)$ -diagrams), due to the effect of dust. The very central region, shown in Fig. 4 is also where the $H\alpha$ gas in emission is detected (Section 3.2). H16d has a second nucleus $\sim 7''$ east of the main nucleus. This double nucleus is uncovered in a K image of the galaxy (Mendes de Oliveira, unpublished). It is not visible in either the R or I bands, due to obscuration by the dust.

The R and I surface brightness profiles can be well described by a $r^{1/4}$ -profile for radii greater than 8'', out to 61'' (at the lowest detectable isophote level of $\mu_R = 25 \text{ mag/arcsec}^2$). A fit to an $r^{1/4}$ -profile gives an effective radius for this galaxy of 10.5 arcsec ($2 \text{ h}^{-1} \text{ kpc}$). The ellipticity and PA profiles are approximately constant for radii between 8'' and 61'' (not plotted) at values of 0.55 and 84° respectively.

H16d shows pointed isophotes, which, at small radii, could be due to the central bar-like structure. However, this pointed morphology dominates the whole structure of the galaxy, and not only its central part, where the bar-like feature is detected.

3.2. $H\alpha$ morphology, kinematics of the gaseous disks and rotation curves

The Data: Figs. 5 to 12 show the monochromatic images, the velocity fields (VFs) of $H\alpha$ and the rotation curves (RCs) for galaxies H16a,b,c and d. The rotational velocities plotted have not been adjusted by the cosmological correction ($1 + z$).

Detailed discussion on the method used to obtain the systemic velocity, center, PA of the major axis and inclination of the galaxy are given in Amram et al. (1996). Advantages of Fabry-Perot observations in the study of galaxy kinematics are also discussed in that paper and in Schommer et al. 1993.

3.2.1. H16a

The pattern of the VF of H16a plotted in Fig. 5 is regular. The grand design of the isovelocity lines describe a normal rotating disk with differential rotation. Morphologically, H16a is a barred galaxy and the signature of the bar is visible in the central parts of the VF. The classical distortions of the isovelocity lines when crossing a spiral arm are clearly seen all along the arms.

The RC of H16a shown in Fig. 6 was plotted taking into account all velocity points except those within 20° of the galaxy minor axis. The cloud of small points represents the portion of measured velocities within $\pm 30^\circ$ of the major axis in the plane of the sky. This gives a fair idea of the quality of our data. The mean RC of H16a (obtained by averaging both sides of the galaxy) is flat from $2''$ to the limit of our measurements at $\sim 30''$. In the outer $5''$ small discrepancies between the two sides occur. These are mainly due to the effects of the spiral arms. The plateau is reached within the inner $0.2 h^{-1}$ kpc-radius. The steep slope (fast rise) of the central RC is a typical signature of a bulgy galaxy.

RHF91 found a peculiar gas velocity pattern for H16a. Outside a radius of $16''$, the rotation curve rises on one side of the galaxy and falls on the other. These points are also plotted on Fig. 6. We do not confirm this result.

We conclude that the RC of H16a is flat out to a $6.5 h^{-1}$ kpc-radius ($0.9 R_{25}$) and that the mass distribution does not seem perturbed by any interaction or merging in the group, inside this radius.

3.2.2. H16b

The $H\alpha$ emission in H16b is very weak and clumpy (see Fig. 7). The monochromatic map and the VF extend to a radius of $\sim 30''$ ($5.8 h^{-1}$ kpc). The total integrated flux is $F(H\alpha) = 0.8 \times 10^{-14}$ erg s $^{-1}$ cm $^{-2}$. The extended emission-line gas lies in a disk of inclination $72^\circ \pm 3^\circ$ and position angle $70^\circ \pm 3^\circ$. These parameters are used to derive the RC plotted in Fig. 8. This plot shows that the rotation curve for H16b is non-axisymmetric. The northeastern side reaches a minimum velocity of -73 km s $^{-1}$ while the southwestern side reaches a maximum velocity of 173 km s $^{-1}$. In the central parts of the galaxy the rotation curve rises very slowly compared to those of other spiral galaxies.

RHF91 obtained a rotation curve for this galaxy, from measurements of the $H\alpha$ and [NII] gas along the photometric major axis. Their results, completely different from ours, are overplotted on Fig. 8. They found that the rotation is in the opposite sense of what we measure. We have re-checked the raw data and have confirmed the sense of rotation. We cannot explain the discrepancy between the results. The RCs derived from the Fabry-Perot maps are based on the average of many more measurements (~ 500 in this case) than for the long-slit determinations.

3.2.3. H16c

The VF and the monochromatic image obtained for H16c were derived from good signal-to-noise data ($S/N \sim 30\text{--}200$), inside a $13''$ -radius. As can be seen from Fig. 9a, the $H\alpha$ emission for H16c is strongly peaked in the central region, although it can be detected out to a $30''$ -radius ($6 \text{ h}^{-1} \text{ kpc}$). The $H\alpha$ flux goes from $32 \times 10^{-14} \text{ ergs}^{-1} \text{ cm}^{-2}$ to $36 \times 10^{-14} \text{ ergs}^{-1} \text{ cm}^{-2}$ if integrated within the $13''$ or the $30''$ -radius. Close to 90 % of the $H\alpha$ -emitting gas mass of the galaxy is within the inner $13''$ radius.

The VF of H16c is reasonably regular, except for the presence of a possible second component to the southwest of the galaxy (Section 3.4). The analysis of the VF of H16c indicates that the extended emission-line gas lies in a disk of inclination $60^\circ \pm 5^\circ$ and position angle $120^\circ \pm 8^\circ$. The morphology of the line-emitting region is decoupled from that of the continuum-light distribution (Fig. 9a). Kinematic decoupling between gas and stars is also observed (Fig. 9b and Section 3.3).

The RC for H16c is plotted in Fig. 10a for a major-axis PA of 120° , an inclination of 60° and the center measured from the VF. The rotation curve resembles that of a gas disk in differential rotation.

The amplitude of the RC of the gas is similar for the receding and approaching sides of the galaxy. The presence of a second gas component does not significantly disturb the shape of the rotation curve as described by the main body of the galaxy (when the center and PA of the major axis are determined from the VF).

In order to compare our results with the result of RHF91, we plotted in Fig. 10b a RC with the center and PA derived from the R image. In that study the photometric major axis of the galaxy was used to position the long-slit. It is clear that along the photometric major axis of the galaxy the shape of the RC is “sinusoidal”, mainly because the second gas component is crossed. Fig. 10b resembles the RC determined by RHF91, from long-slit spectroscopy of the gas in emission. A detailed discussion of Fig. 10 is in Section 4.1.

3.2.4. H16d

The emission in H16d is much less extended than for the other three galaxies and also strongly peaked. The monochromatic map and the VF (plotted in Fig. 11) extend to radii of $\sim 10''$ and $\sim 6''$ respectively. Analysis of the VF of H16d indicates that the gas lies on a disk of inclination $47^\circ \pm 5^\circ$ and position angle $70^\circ \pm 8^\circ$. These parameters are used to build the RC shown in Fig. 12. This RC shows an extension of only $\pm 5''$ on each side of the galaxy. The maximum velocity is $110 \pm 7 \text{ km s}^{-1}$, reached after $5''$ ($1 \text{ h}^{-1} \text{ kpc}$). In the northeast side, the curve reaches a maximum and then falls to about $60 \pm 5 \text{ km s}^{-1}$. This side of the curve may be affected by the presence of a second nucleus, $7''$ east of the bright central nucleus. In Fig. 11 the position of the second nucleus is indicated in both pannels by a cross.

3.3. Misalignment between gas and stars and kinematic warps

H16c displays the largest misalignment between the kinematic axis inferred from the gas motions and the photometric (major) axis measured from the stellar light (40°) followed by H16b (16°) and H16d (14°). For H16a the kinematic and stellar axes are aligned.

The major axis of H16c was measured from the H α image, the VF, the continuum and R images (Table 2 contains derived quantities for all four of the H16 galaxies). The value of $115^\circ \pm 10^\circ$, determined from the monochromatic image, is very similar to that defined by the overall kinematics of the main body of the galaxy determined from the VF ($120^\circ \pm 8^\circ$, see Fig. 9b). These are, however, very different from the major axis defined by the stars, as derived from the continuum, R and I images ($80^\circ \pm 5^\circ$), implying a misalignment of $\sim 40^\circ$ between the stellar and gaseous major axes.

H16c also has an offset between its gaseous kinematic center and the bright optical center. The kinematic center (shown with a “+” in Fig. 9b) lies about $6''$ ($1.2 \text{ h}^{-1} \text{ kpc}$) to the north of the brightest nucleus (also shown with a “+”). The kinematic major axis is placed at the axis of symmetry of the main kinematic body (see Fig. 9b). The center of the VF is chosen to be a point along the major axis which makes the rotation curve symmetric (with similar amplitudes for the receding and approaching sides).

Misalignment between the kinematic and photometric major axes is also detected for H16d, but in this case of only $\sim 14^\circ$ (see Fig. 11b). For H16b the major axis determined from the velocity field is $70^\circ \pm 10^\circ$, different from the stellar major axis by $\sim 16^\circ$ (see Fig. 7b).

H16 b and c display strong kinematic warping, i.e. variation of the position angle of the kinematic major axis with radii. H16b presents a 60° change of the PA of the major axis between a radius of $9''$ and $27''$. The kinematic major axis of the main component of H16c shows a PA variation of over 60° along the galaxy. No variation of the PA of the major axis with radius was detected for H16 a and d.

3.4. Possible second component in H16c

The 3900 kms^{-1} iso-velocity contour in the southwest region of the VF of H16c is not consistent with the rest of the map (see Fig. 9). This component is derived from profiles with $S/N = 90 \text{ pixel}^{-1}$. It is therefore not an artifact of the data. In order to show that this component is caused by noncircular gas motions we plot in Fig. 13 the observed radial velocity at some given projected distance from the kinematic center of rotation of the galaxy as a function of the PA of the major axis. Plots for three values of projected distance from the center, 5, 10 and 15 arcsec are shown. A clear deviation from a smooth curve occurs between PAs 220° and 280° , due to the presence of a second gas component.

3.5. Velocity-dispersion measurements

The width of the emission-line profiles of the galaxies are used to measure the velocity dispersion of the ionized gas. In the determination of the full-width of half maximum (fwhm) of the emission-line profiles, we checked if velocity gradients in the galaxies, low-S/N ratio of the data, instrumental profile and seeing effects were artificially biasing the results. First the non-smoothed data were analyzed and the instrumental profile (fwhm of $\sim 36 \text{ km s}^{-1}$) was used to deconvolve the data. Where the S/N was too low, some smoothing had to be done and the process reiterated. At the distance of H16 one pixel is a square of $200 h^{-1} \text{ pc}$ on a side.

The fwhm of the profiles in the center of H16a is $125 \pm 10 \text{ km s}^{-1}$ and $80 \pm 10 \text{ km s}^{-1}$ in the region of the spiral arms. For H16c, the fwhm of the profiles in the central region is $\sim 130 \pm 10 \text{ km s}^{-1}$ dropping quickly to $\sim 90 \pm 10 \text{ km s}^{-1}$ to the east and south-east of the galaxy. For H16d, the fwhm is $\sim 145 \pm 15 \text{ km s}^{-1}$ in the central 5 arcsec and decreasing quite rapidly but regularly to $\sim 30 \pm 5 \text{ km s}^{-1}$ at $10''$ from the center. These results are summarized in Table 2. The low S/N for the H16b data cube did not allow the determination of meaningful values of the fwhm for this galaxy.

3.6. Mass determinations

The mass determinations are summarized in Table 2. They were derived for an adopted H_0 of $75 \text{ km s}^{-1} \text{ Mpc}^{-1}$ and a distance to the group of 51.35 Mpc. We describe below how the values in Table 2 were obtained.

Treating non-circular motions as negligible perturbations, the mass of a spiral galaxy out to a certain radius can be estimated from the rotational velocity of the disk using the circular approximation. We estimated the total masses of the galaxies within a given radius following Lequeux (1983).

The “warm” ($H\alpha$ -emitting) gas mass was obtained from the formula given by Osterbrock (1974, case B recombination): $M_{HII} = 2.8 \times 10^{-3} D^2 F(H_\alpha) n_e$, where D is the distance to the group in Mpc, $F(H_\alpha)$ is the total flux within a given radius and n_e is assumed to be 1000 cm^{-3} . This may overestimate the gas mass, given that the value assumed for n_e is an upper limit. In the presence of dust, however, this may underestimate the warm-gas mass.

The dust mass was obtained using the values from Allam et al. 1996 for the IRAS fluxes in 60μ and 100μ . We used the formula from Young et al. (1989) to calculate the dust mass, with the assumptions and approximations made by Roberts et al. (1991, their formula 7).

The values for the X-ray emission in H16c and d are taken from Saracco et al. (1995). The formula (4) given by Roberts et al. (1991) was used to derive an X-ray gas mass for these galaxies.

Based on independent measurements at several different wavelengths, H16c and H16d contain

significant amounts of interstellar matter. The gas mass for H16c is about 6% of the total mass of the galaxy inside a radius of $\sim 0.9 R_{25}$.

4. General discussion of the results

Each of the four HCG 16 galaxies shows various evidences for interactions. This is clearly a very high density group. This gives an excellent opportunity to correlate the different galaxy properties suggested to be induced by galaxy-galaxy interactions. Via comparison with the recent simulations of interacting galaxies, we can also attempt to characterize the type of interaction each of the HCG 16 galaxies has undergone and to trace the interaction history of the group. Before discussing these principal results of the study, we address three other issues: the previous claims of unusual rotation curves for these galaxies, how these galaxies fit onto the Tully-Fisher and Fundamental Plane relations and the presence of dwarf galaxies in the tidal tails of H16a.

4.1. Falling and/or sinusoidal rotation curves?

RHF91 presented evidence that a large fraction of the compact-group spirals have falling rotation curves, unlike field spirals. If falling rotation curves are common in compact groups, this would suggest that the individual dark matter halos are absent most probably because they were stripped by interactions. In particular both H16c and H16d were reported to have sinusoidal RCs, from measurements of the kinematics of the gas obtained through long-slit spectra taken along the photometric major axis of the galaxies. Having the 2-D VFs of the galaxies we can check on the reality of the sinusoidal shapes of the RCs.

Fig. 10 shows two possible RCs for H16c (described in Section 3.2.3). Fig. 10b was built with the same parameters used by RHF91, i.e., $PA=78^\circ$ and the center coinciding with the optical/continuum center. This curve clearly has a sinusoidal shape, in agreement with the curve presented in RHF91.

The rotation curve of H16c plotted using the kinematical center, inclination and position angle (Fig. 10a and see §3.3 for how these quantities are defined and derived) has a fairly normal shape typical of a disk in differential rotation. The sinusoidal rotation curve derived through long-slit spectroscopy (Fig. 10b) along the photometric major axis of H16c was caused by a misalignment between the gas and stellar components and the presence of a second kinematic component.

There are a number of merger-candidates in the literature previously found to have sinusoidal rotation curves. It would be interesting to review these cases with a full 2-D velocity field analysis (e.g. Mihos & Bothun 1998, Hibbard et al. 1996).

In the case of H16b and H16d it is not possible to make their rotation curves look normal by changing the center or the position angle along which the curve is plotted. H16b has the

peculiarity of having one side (the northeast) with a much lower velocity amplitude than the other side, while for H16d the velocity curve reaches a maximum and drops on both sides.

4.2. The Tully-Fisher and the fundamental-plane relations

Dynamical processes may have worked very efficiently in HCG 16, as exemplified by the high frequency of interaction indicators found for all member galaxies. It is of interest to investigate if the “damage” due to interactions and merging was large enough to affect the position of the galaxies in the Tully-Fisher or fundamental-plane relations.

In order to check if H16a, H16c and H16d follow the TF relation we have used the plots in Figs. 6, 10 and 12 to estimate the shape and amplitude of the rotational velocity curves and we have then compared these with “template curves” based on the TF relation for normal galaxies (RHF91, Fig. 5). No attempt is made to check if H16b follows the TF relation since the two sides of its rotation curve do not coincide. H16a has a normal velocity amplitude for its luminosity, following the TF relation. For the main disk component of H16c the measured V_{max} is also within the expected value, for a galaxy of this luminosity (see Fig. 5 of RHF91 and table 2). A similar exercise, for H16d shows that V_{max} is ≤ 0.5 of the value expected for a normal galaxy of this luminosity, if the inclination given by the velocity field (inclination = 47°) or R image (inclination= 57°) is used. There is a chance, however that the flattening of the velocity curve for H16d is due to dust. Alternatively there could be problems in obtaining dynamical information about gravity from the measured gas properties in the inner 5 " of an interacting galaxy. Dynamical information from the stars would be much more reliable in this case.

The surface-brightness of H16d follows an $r^{1/4}$ -profile, typical of early-type galaxies. It is, therefore, of interest to check if it follows the r_{eff} vs. μ_{eff} relation, a projection of the fundamental-plane relation, observed for bulges and elliptical galaxies. With the values of $r_{ref} = 10.5$ and $\mu_{eff} = 21.1$ mag arcsec $^{-2}$, we find that H16d follows the fundamental plane relations of normal field galaxies (Kormendy & Djorgovski 1989).

4.3. Dwarf galaxies in tidal debris ?

The analysis of R images of Hickson compact groups by Hunsberger et al. (1996) yielded a sample of 47 candidate dwarf galaxies that may be associated with tidal arms and tails in interacting and merging galaxies. If the majority of these dwarf-galaxy candidates are confirmed as being gravitationally bound stellar systems, these authors estimated that a significant fraction (perhaps as much as one-half) of the dwarf population in compact groups is created in mergers occurred in the giant parent galaxies.

Three dwarf candidates are suggested by Hunsberger et al. (1996) to sit on the eastern tail

of H16a. Two of the candidates were observed in our fields. We checked if emission lines are associated to the candidates. In both cases, the emission-line map has a S/N twice higher on the corresponding pixels than in the direct neighbourhood of these pixels. We therefore confirm these may be star-forming knots at the redshift of the group. However, no conclusive information can be obtained from the examination of the velocity field, the line-width and the equivalent-line-width maps, due to insufficient S/N. We conclude that the “dwarf candidates” are at the same redshift of the group but we cannot exclude the possibility that they are material connected to the main galaxies. Longer exposure and higher spatial resolution are necessary to confirm the nature of the emission, if these are galaxies formed in interactions or just part of the main galaxy which will fall back in a few crossing times.

It is interesting to note that these star-forming knots are found exactly in the galaxy for which we show that no merging has occurred (H16a).

4.4. A census of the interaction-related properties for the H16 galaxies

There are a number of “interaction indicators” that have been suggested over the years. These have been used to attempt to discern the different types of interactions (primarily tidal interactions vs. merging) that can occur between galaxies and are generally based on models of colliding systems.

Table 3 lists eight interaction/merging indicators and whether or not each is seen in the four galaxies of H16.

Close tidal encounters which do *not* lead to merging can strongly affect the interstellar medium of the colliders, can trigger strong bursts of star formation on a timescale of a few 10^8 years but can only mildly affect the *kinematics* of the central velocity fields of the colliding galaxies. In a merger, on the other hand, even if the two nuclei have not yet mixed completely, the regular kinematic structure of the disks disappear and the velocity fields may display strong signatures of the collision (e.g. the Antennae galaxies, Amram et al. 1992, N7252, Hibbard et al. 1996). We, therefore, use the indicator “highly disturbed velocity field” as one of our definite evidences for a merger. Central double nuclei and/or double kinematic gas components are other definite indicators of mergers. Double nuclei are present, for example, in the well known mergers, the Antennae galaxy (Amram et al. 1992), N520 (Hibbard et al. 1996) and IRAS 23128-5919 (Mihos & Bothun 1998) and double kinematic gas components are present in IRAS 23128-5919, the Cartwheel galaxy (Amram et al. 1998), HCG 31 and several other obvious merger candidates.

We list as interaction indicators for collisions which do not necessarily lead to merging the following properties: kinematic warping, gaseous and stellar major axes misalignments, tidal tails, high infrared luminosity and central activity. Although the presence of tidal tails and plumes are common in mergers and they are often taken as evidence for a major accretion event, we group it with the indicators of mild interaction since they can also be formed in interactions which do

not lead to mergers. Kinematic and photometric major axes misalignment and kinematic warping are properties that are also usually associated with galaxy collisions. In a sample of 75 normal spiral galaxies studied by Schommer et al. 1993, for which velocity fields were available, only a very small fraction of the galaxies showed kinematic warping and/or small gaseous/stellar major axes misalignments. Another indicator listed in Table 3 is “high infrared luminosities”. Certainly not all strongly interacting galaxies have high IR luminosities but most IR loud galaxies have disturbed morphologies. Finally, “central activity” is taken as an interaction indicator. Although there is not a one-to-one correlation between interactions and central activity, there are several lines of evidence that strongly suggest that interactions may drive nuclear inflows and fuel central activity in interacting systems.

4.5. The interaction history of the H16 galaxies

The data presented in this paper support the existence of a regular gaseous rotating disk in the center of galaxies H16a, b, c and d. H16c may contain two disks. Based on the interaction indicators for each galaxy listed in Table 3 and in the context of the various models of galaxy interactions (Barnes 1989, Barnes & Hernquist 1992, Barnes & Hernquist 1996) we suggest the following histories for the H16 galaxies.

H16a: This galaxy does not present any of the indicators common to merging galaxies, listed in Table 3. It has a normal mass distribution inside a radius of 30 arcsec and it does not contain any multiple nuclei or gas components. At large radii, however, the galaxy looks morphologically disturbed and shows tidal tails to the east and south. Although numerical models of compact groups suggest that galaxies with extended tidal tails are excellent candidate mergers (Fig. 1 of Barnes 1989), the grand-design isovelocity lines of H16a with no signs of disturbances inside a radius of $\sim R_{25}$ strongly suggest that this galaxy has not yet suffered a major merger.

An interaction between galaxies H16a and H16b is very probable. The difference in systemic velocities between these two galaxies is less than 200 km s^{-1} and their isophotes overlap. The normality of the velocity field of this galaxy compared with the peculiarities observed for the velocity fields of the other three very kinematically disturbed companions, leads us to the conclusion this may be a fairly new member to the heart of the group.

H16b: Although H16b is classified as an Sb galaxy, it has a velocity field which is very peculiar, unlike that observed for any other normal spiral galaxy (e.g. Schommer et al. 1993). Strong warp of the kinematic major axis, misalignment between the optical and kinematic axes and a very slow rise in the velocities in the inner regions of the galaxies are obvious peculiarities related to past or ongoing interactions. In addition, the blue and red sides of its velocity curve do not match in shape nor in amplitude and its visual morphology is asymmetric, although smooth and “well behaved” (if compared with the morphologies of other merger remnants). The close proximity of H16a and the overlapping isophotes with this galaxy suggest a clear ongoing

interaction. H16b has little ionized gas compared to the other members of the group studied here (Table 2). Also the mass of molecular gas is four times smaller than the average value for the other members. It is the one galaxy from the four studied here that is not detected at radio or infrared wavelengths. Although H16b does not show a double nucleus or a double gas system, which would be a clear sign of an ongoing merger, the very disturbed velocity field calls for a scenario where strong interactions or accretion events have occurred in the past, which have, however, left the disky morphology of the galaxy intact. A gas-poor accretion event is possible, given the lack of gas in H16b. The scarcity of gas and consequent low S/N of the data did not allow detection of a double gas component, if it was present. In addition to having suffered accretion events H16b may be involved in an on-going interaction with H16a, which may result in a major merger. Unlike the two ongoing mergers in H16 (H16c and H16d, see below) the warm gas content of H16b is not concentrated to the center of the galaxy.

H16c: This galaxy is clearly an ongoing starburst merging system. It presents seven indicators (all but “tidal tails”) for strong interactions and mergers, according to Table 3. The VF of H16c shows the existence of a second velocity component to the southwest of the galaxy, closely spaced in velocity and position to the main component. The observed kinematic warp and misalignment between gas and stars are strong evidences for external accretion of the central ionized gas in H16c. Its infrared luminosity is comparable to that of other mergers ($\log L_{IR} = 11.6 L_{\odot}$). The morphology of the galaxy as a whole is amorphous. No disks or spiral arms or tails are seen down to a surface brightness limit of $R = 25 \text{ mag arcsec}^{-2}$. The shapes of the continuum and monochromatic images of H16c (Fig. 4) indicate that the emission-line isophotes are significantly flatter than the isophotes of the underlying stellar component, typical of early-type galaxies. However, the light profile of the galaxy does not follow an $r^{1/4}$ law as is common for relaxed mergers.

The kinematics of H16c resembles that of the merger remnant N6240 (Bland-Hawthorn et al. 1991). The overall optical morphology of H16c, however, is much less peculiar than that of N6240 or of any other ongoing merger remnant from the Toomre and Toomre’s sequence. It is possible that pre-existing tidal arms or tails were quickly ripped apart by the dynamical forces within the compact group, a situation which is unlikely to happen in less dense environments (Barnes & Hernquist 1992). Alternatively tidal tails may have never been formed.

The HI map of the group (Williams, private communication) shows a strong connection between galaxies H16c and H16d. It also shows that the centers of the HI contours are displaced from the optical centers of H16c and H16d by almost one optical radius, in the direction of the line that joins the centers of these two galaxies.

H16d: This galaxy may also be a merger remnant. It presents five of the eight indicators of interactions and mergers, from Table 3. Double kinematic gas component, kinematic warping and tidal tails are not detected for this galaxy. The first two indicators are not observed probably due to the small range in radii where the gas kinematics can be measured. The lack of tidal tails is

common to all mergers in group H16 and may be a common feature of mergers in compact groups in general.

H16d has a double nucleus and a peculiar velocity field. It has a high infrared luminosity ($\log L_{IR} = 11.7 L_{\odot}$), similar to that of other mergers. Outside a radius of 8 arcsec the light profiles of the galaxy (in the R and I bands) follow an $r^{1/4}$ -profile with an r_{eff} of 10.5 arcsec. In the inner parts the galaxy profiles flatten, as is typical of the mass profiles of modeled merger remnants (eg. Barnes 1992). H16d has a peculiar bar-like structure in the central $10''$ which coincides with the peaked ionized gas, molecular gas and dust components. The rotation curve of H16d peaks and falls on both sides within the inner $2 h^{-1}$ kpc region. We do not have kinematical information on the second nucleus, which lies 7 arcsec to the east of the main nucleus. The second nucleus is only seen in the NIR due to obscuration from dust in the optical. The $H\alpha$ emission in H16d (and in H16c also) is strongly spatially concentrated, in qualitative agreement with the results of simulations of gaseous collisions, in which the gas is driven towards the nucleus of the galaxies (e.g. Barnes & Hernquist 1996).

Our measurements support the models of dynamical evolution of compact group galaxies (Barnes 1992) and should impose strong constraints to the detailed simulations of the gas kinematics during group merging.

The authors thank Barbara Williams for providing an HI map of H16, Chantal Balkowski, Roger Coziol and Jacqueline van Gorkom for insightful discussions and J.L. Gach for helping during the observations. CMdO acknowledges the financial support from the Alexander von Humboldt foundation. H. Plana acknowledges the financial support of the Brazilian FAPESP, under contract 96/06722-0.

Table 1. Journal of Perot-Fabry observations

Compact Group of Galaxies HCG 16		
Observations	Telescope	ESO 3.6m
	Instrument	CIGALE @ Cassegrain focus
	Date	August 26 th and 27 th 1995
	Seeing	~1"
Interference Filter	Central Wavelength	6653 Å ¹
	FWHM	24 Å ²
	Transmission	0.70/0.69/0.65/0.65 ^{1,3}
Calibration	Neon Comparison light	λ 6598.95 Å
Perot-Fabry	Interference Order	796 @ 6562.78
	Free spectral range at Hα (km s ⁻¹)	387.7
	Finesse	12 at Hα
	Spectral resolution at Hα	9600
Sampling	Number of Scanning Steps	24
	Sampling Step	0.36 Å (16.15 km s ⁻¹)
	Total Field	230" × 230" (256 × 256 px ²)
	Pixel size	0.91"
Detector	Photon Counting Camera (IPCS)	Time sampling of 1/50 s
Exposures times	Total exposure	2 hours per field
	Elementary scanning exposure time	5 s per channel
	Total exposure time per channel	300 s

¹ For a temperature of 5°

² For a mean beam inclination of 2.7°

³ Transmission for the mean redshift of H16a,b,c and d respectively

Table 2. General and physical parameters for the H16 galaxies

Name	HCG 16a	HCG 16b	HCG 16c	HCG 16d
Other Names	N835/Mrk 1021	N833	N838/Mrk 1022	N839
α (1950) ¹	02 ^h 06 ^m 57.4 ^s	02 ^h 06 ^m 53.3 ^s	02 ^h 07 ^m 11.3 ^s	02 ^h 07 ^m 15.6 ^s
δ (1950) ¹	–10°22'20.0"	–10°22'08.9"	–10°22'56.0"	–10°25'11.1"
Morphological type ^{1,2}	SBab/SBab	Sab/Sa	Im/SO(pec)	Im/SO(pec)
Systemic Velocity (km s ^{–1}) ^{1,3}	4152/4052	3977/3837	3851/3858	3847/3864
D(Mpc) $H_o = 75 \text{ km s}^{-1} \text{ Mpc}^{-1}$	51.35	51.35	51.35	51.35
B_T (mag) ¹	12.7	13.2	13.1	13.4
$D_{25}/2$ (") ²	37±10	45±7	34±10	43±4
Fluxes and masses of the different ISM components				
F(H α)10 ^{–14} erg s ^{–1} cm ^{–2}	12.8	0.8	36.0	20.0
Log L(H α) erg s ^{–1}	39.5	38.3	40.0	39.7
M_{HII} (10 ⁴ M \odot)	9.4	0.6	26.5	14.7
M_{tot} (10 ¹⁰ M \odot)/ R_{max} (h ^{–1} kpc)	8.3/6.3	4.3/6.7	7.2/7.5	0.23/1.1
M_X (10 ⁸ M \odot)	28.8 ⁴		9.1	6.6
M_{H_2} (10 ⁹ M \odot) ⁵	2.4	0.6	2.6	1.9
M_{Dust} (10 ⁷ M \odot)	1.07	< 0.04	1.5	1.7
Major-axis position angles (this study)				
Velocity Field	3°± 10°	70°± 3°	120°± 8°	70°± 8°
Monochromatic Map	0°± 10°	86°± 10°	115°± 10°	80°± 7°
Optical Image	3°± 5°	86°± 10°	80°± 5°	84°± 5°
Inclination of the disk (this study)				
Velocity Field	43°± 5°	72°± 3°	60°± 5°	47°± 5°
Continuum image	57°± 5°	58°± 5°	48°± 8°	27°± 7°
R image (at R ₂₅)	38°± 8°	66°± 8°	44°± 8°	57°± 5°
Parameters from the gas VF and Rotation Curves (this study)				
Systemic Velocity (km s ^{–1})	4040	3905	3850	3845
Min. velocity (projected, km s ^{–1})	–163	–77	–220	–78
Max. velocity (projected, km s ^{–1})	174	183	225	76
FWHM of central profiles (km s ^{–1})	125		130	145

¹ from Hickson (1993)

² from de Vaucouleurs et al. (1991)

³ from RHF91

⁴ mass is given for H16A+B

⁵ from Boselli et al. (1996)

Table 3. Interaction indicators

	HCG 16a	HCG 16b	HCG 16c	HCG 16d
Highly disturbed velocity field ¹	–	+	+	+
Central double nuclei ¹	–	–	+	+
Double kinematic gas component ¹	–	–	+	–
Kinematic warping ²	–	+	+	–
Gaseous <i>vs.</i> stellar major axis misalignment ²	–	+	+	+
Tidal tails ²	+	–	–	–
High IR luminosity ²	+	–	+	+
Central activity ²	+	+	+	+

¹ Indicator definitely associated with mergers

² Indicator does not require that a merger has occurred

REFERENCES

- Allam S., Assendorp R., Longo G., Braun M., Richter G., 1996, *A&AS*, 117, 39
- Amram P., Mendes de Oliveira C., Boulesteix J., Balkowski C., 1998, *A&A*, 330, 881
- Amram P., Balkowski C., Boulesteix J., Cayatte V., Marcelin M., Sullivan W.T. III, 1996, *A&A*, 310, 737
- Amram P., Marcelin M., Boulesteix J., le Coarer, E., 1992, *A&A*, 266, 106.
- Barnes J., 1992, *ApJ*, 393, 484
- Barnes J., 1989, *Nature*, 338, 123
- Barnes J., Hernquist L., 1996, *ApJ*, 471, 115
- Barnes J., Hernquist L., 1992, *ARA&A*, 30, 705
- Bland-Hawthorn J., Wilson A., Tully B., 1991, *ApJ*, 375, 19
- Boselli A., Mendes de Oliveira C., Balkowski C., Cayatte V., Casoli F., 1996, *A&A*, 314, 738.
- Boulesteix J., 1993, "ADHOC reference manual", Publications de l'Observatoire de Marseille.
- Coziol R., Ribeiro A.L.B., de Carvalho R.R., Capelato H.V. 1997, *ApJ*, 493, 563
- de Vaucouleurs G., de Vaucouleurs A., Corwin, H.G. Jr., Buta, R.J., Paturel G., Fouque, P. 1991, *Third Reference Catalog of Bright galaxies*, Springer-Verlag (RC3).
- Hibbard, J.E., van Gorkom, J.H., 1996, *AJ*, 111, 655
- Hickson P., 1982, *ApJ*, 255, 382.
- Hickson P., Auman J., Kindl E. , 1989, *ApJS*, 70, 687.
- Hickson P., Mendes de Oliveira C., Huchra J.P., Palumbo G.G.C., 1992, *ApJ*399, 353.
- Hickson P., 1993, *Astrophys. letters & Communications* Vol 29 numbers 1-3
- Hunsberger S.D, Charlton J.C., Zaritsky D., 1996, *ApJ*, 462, 50
- Jedrzejewski R.I, 1987, *MNRAS*, 226, 747
- Kormendy, J., Djorgovski, S. 1989, *ARA&A*27, 235
- Laval A., Boulesteix J., Georgelin Y.P., Georgelin Y.M., Marcelin M., 1987, *A&A*, 175, 199.
- Lequeux J., 1983, *A&A*, 125, 394.

Menon T.K., 1995, MNRAS, 274, 845.

Mihos J.C., Bothun G.D. 1998, ApJ, preprint

Osterbrock D.E., 1974, Astrophysics of Gaseous Nebulae (W.A. Freeman and Company, San Francisco) p 71

Ponman T.J., Bounder P.D.J., Ebeling H., Bohringer H., 1996, MNRAS, 283, 690.

Ribeiro A., de Carvalho R., Coziol R., Capelato M., 1996, ApJLetters, 463, L5.

Roberts M.S., Hogg D.E., Bregman J.N., Forman W.R., Jones C., 1991, ApJS, 75, 751

Rubin V., Hunter D., Ford JR., 1991, ApJS, 76, 153 (RHF91)

Saracco P., Ciliega P., 1995, A&A, 301, 348.

Schommer, R.A., Bothun, G.D., Williams, T.B., Mould, J.R., 1993, AJ, 105, 97.

Young J., Xie S., Kenney J., Rice W., 1989, ApJS70, 699

Fig. 1.— Continuum contour plots superimposed on the I image of H16. North is up; east is to the left. The two squares (230" on a side) indicate the field of view of the Fabry-Perot instrument for the two observed frames. The I-image is 7.7' on a side. The continuum contours are plotted in a linear arbitrary scale.

Fig. 2.— R image of the inner regions of H16 c and d. The box around each image is 12-arcsec on a side. North is up and east is to the left. The center of the concentric-elliptical isophotes outside a radius of 10 arcsec is placed in the middle of the box. Elliptical isophotes with a major-axis radius of 5 arcsec ($\sim 1 \text{ h}^{-1} \text{ kpc}$) are draw on the figures for guidance on the scale only. Left image, H16c: the double nucleus is not coincident with the center of the main body of the galaxy, as described by its outer isophotes and kinematics. Right image, H16d: the galaxy has an inner high surface brightness nucleus with a bar-like feature within its inner 5" radius.

Fig. 3.— Surface brightness profiles of H16c obtained for the gas component (closed circles), and stars (open circles). The top label and axis correspond to the two curves on the right of the plot (fits to an $r^{1/4}$ -profile) while the bottom label and axis relates to the two curves on the left of the diagram (linear fits). The vertical normalization is done arbitrarily. The profiles are not well fit by an $r^{1/4}$ or linear profile. It is evident, however, that the slope of the monochromatic profile (gaseous component) is much steeper than the slope of the continuum image (stellar component) outside a radius of 5 arcsec. This is typical of gaseous disks in elliptical and lenticular galaxies.

Fig. 4.— Surface brightness, ellipticity, position angle and $\cos(4\theta)$ profiles for H16d in R (X) and I (open circles) See text for details.

Fig. 5.— H16a – Upper-left: continuum iso-intensity contours in a linear arbitrary scale. Bottom-left: monochromatic iso-intensity map, calibrated in units of $10^{-17} \text{ ergs}^{-1} \text{ cm}^{-2} \text{ arsec}^{-2}$. The lowest level is 0.65 and the step is 2.6. Right pannel: Isovelocity contours of the ionized gas (thick solid lines) are superimposed on the monochromatic image (thin solid lines). The heliocentric radial isovelocity lines have been drawn after smoothing of the original profiles with a gaussian function (of fwhm $1.5'' \times 1.5''$).

Fig. 6.— Rotation curve obtained from both sides of H16a. The cloud of points represents the portion of measured velocities within $\pm 30^\circ$ of the major axis in the plane of the sky. The large velocity points are weighted averages for the entire data set (within $\pm 70^\circ$ of the major axis PA) over successive concentric annuli in the plane of the galaxy. The weights are proportional to $\cos \theta$, where θ is the angular separation of a pixel from the major axis as measured in the plane of the galaxy. For each annulus we give the average velocity for the receding side (\otimes), the approaching side (\odot), and the average of both sides (small filled circle), with a ± 1 rms error bar. Points enclosed within parentheses () are derived from only one or two measured velocities. The final rotation curve (thick solid line) is a cubic spline function least-square fitted to the average points, weighted by their errors. The large squares (\square) plot the rotation points of RWF adopting our inclination (The size of the square is roughly the mean error adopted by RHF91). The receding side is showed

by an “X” within the square and the approaching side by a point within the square. A value of $H_0 = 75 \text{ km s}^{-1} \text{ Mpc}^{-1}$ has been adopted for the distance scale. The arrows along the abscissa indicate the $0.4R_{25}$ and $0.8R_{25}$. Small crosses are plotted on the fitted RC at these abscissae. R_{25} is the corrected radius at the 25th magnitude arcsec^{-2} isophote, as given in Table 2 ($D_{25}/2$).

Fig. 7.— (a) Monochromatic image for H16b, calibrated in units of $10^{-18} \text{ erg s}^{-1} \text{ cm}^{-2} \text{ arcsec}^{-2}$. The lowest level is 3 and the step is 1.5. The continuous line represents the stellar major axis which is coincident with the major axis defined by the morphology of the gas. (b) Velocity field built from the $\text{H}\alpha$ line emission. The two continuous lines represent the stellar major axis (same as in Fig. 7a) and the major axis defined by the kinematics of the gas.

Fig. 8.— Rotation curve for H16b (PA=70°). The crosses are weighted averages within 30° of the kinematic major axis PA. Filled circles represent the mean radial velocities. RHF91’s data are overplotted as open triangles.

Fig. 9.— (a) The monochromatic iso-intensity map for H16c, calibrated in units of $10^{-17} \text{ erg/s/cm}^2/\text{arcsec}^2$. The lowest level is 0.7 and the step is 20. The two continuous lines, represent the stellar (SA) and gas (GA) major axes. The intersection of these two lines mark the monochromatic center. (b) The velocity map built from the $\text{H}\alpha$ -line emission. The upper and lower crosses represent the kinematical and continuum centers respectively.

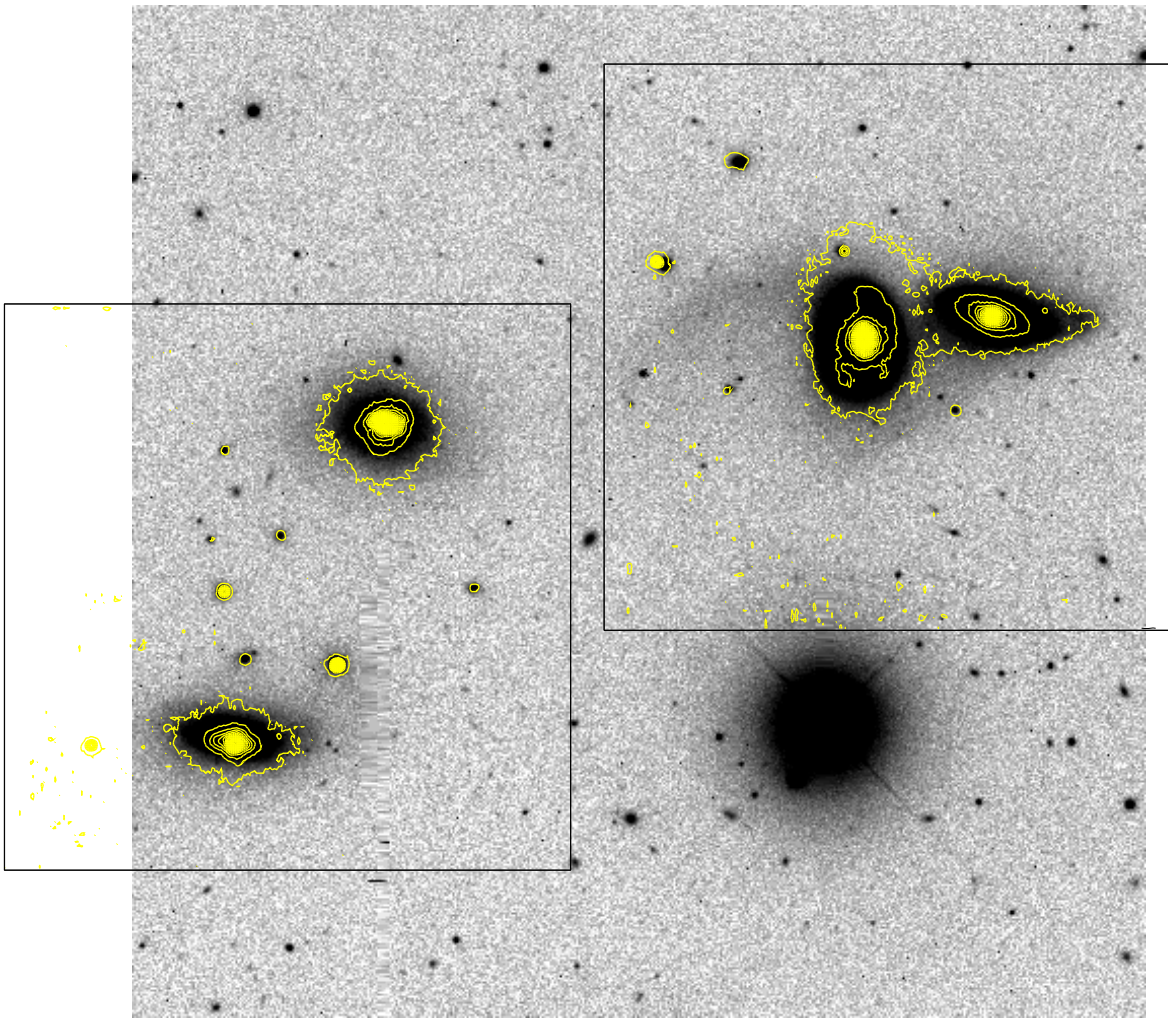
Fig. 10.— Rotation curve for H16c: (a) Crosses represent all measured values within 40° of the kinematic major axis (PA=120°). The center is taken to be the kinematic center. The solid dots represent the average velocities. (b) Crosses and solid dots as in Fig. 10a, but for a major axis with PA=78° and with the continuum center. Overplotted are the velocities measured by RHF91 as open triangles. See text for details.

Fig. 11.— (a) The monochromatic iso-intensity map for H16d, calibrated in units of $10^{-17} \text{ ergs}^{-1} \text{ cm}^{-2} \text{ arcsec}^{-2}$. The lowest level is 0.7. and the step is 10. The small cross marks the monochromatic center of the galaxy. The continuous line marks the gas major axis, measured from the morphology of the monochromatic image (GA, which is almost coincident with the stellar axis - see Table 2). (b) The velocity field built from the $\text{H}\alpha$ -line emission. The small cross represents the kinematic center. The two continuous lines mark the kinematic (GA) and stellar (SA) major axes. In both pannels the large cross, 7" to the east of the main center, indicates the position of the second nucleus of the galaxy (see section 3.1).

Fig. 12.— Rotation curve for H16d. De-projected velocities are plotted for two values of major axis position angles, that determined from the velocity field of HCG 16d (70°, solid dots) and the PA obtained by RHF91 from the photometry of the galaxy (86°, open diamonds). Overplotted as open triangles are the velocities measured by RHF91 along the photometric major axis of the galaxy.

Fig. 13.— Heliocentric radial velocity *vs.* position angle for H16c, for three different values of r , where r is the distance to the center of the galaxy. The effect of a possible second gas component

is seen between PAs 220° and 280° .



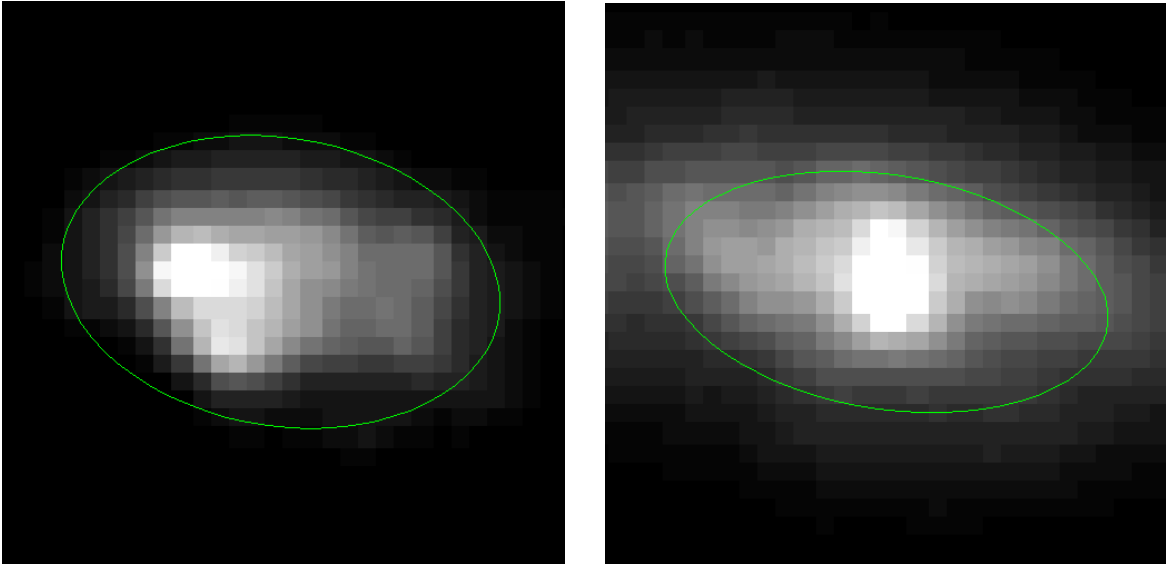


Fig. 2

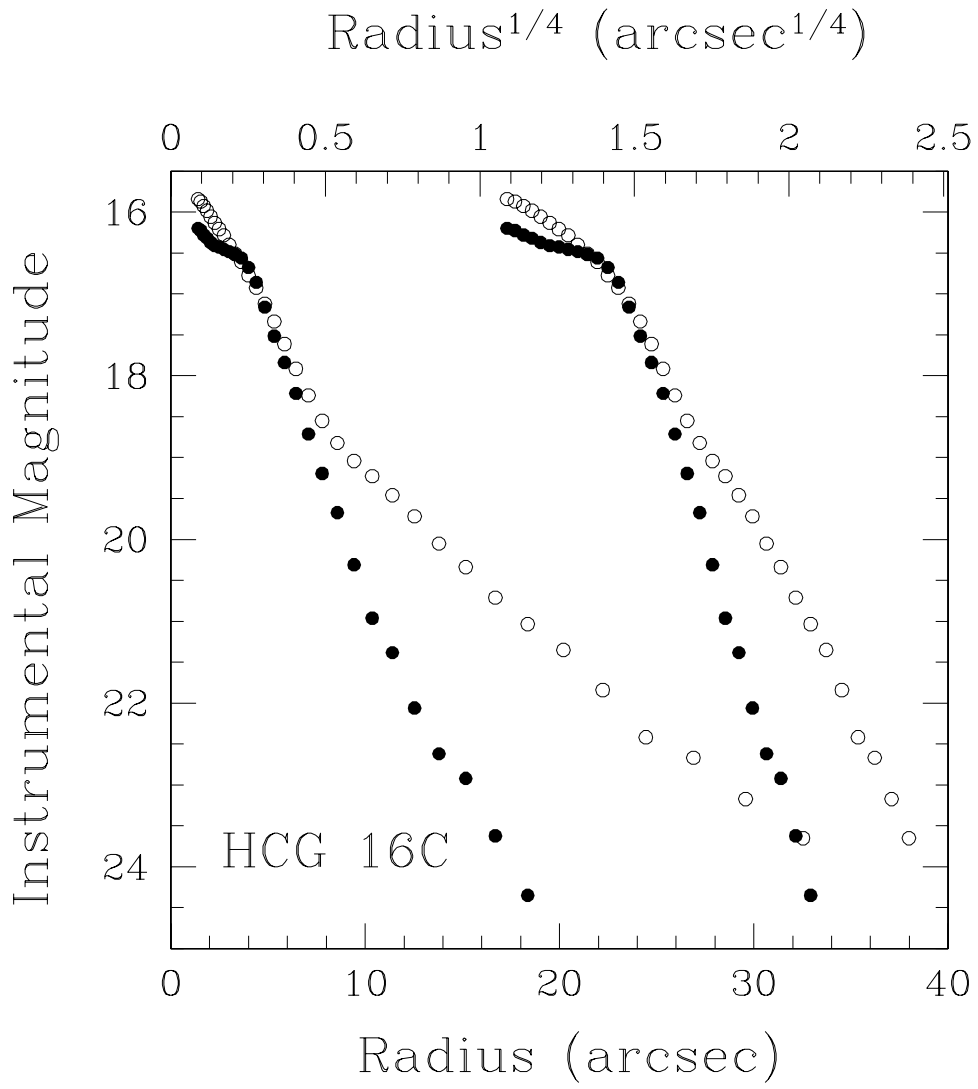


Fig. 3

H16d

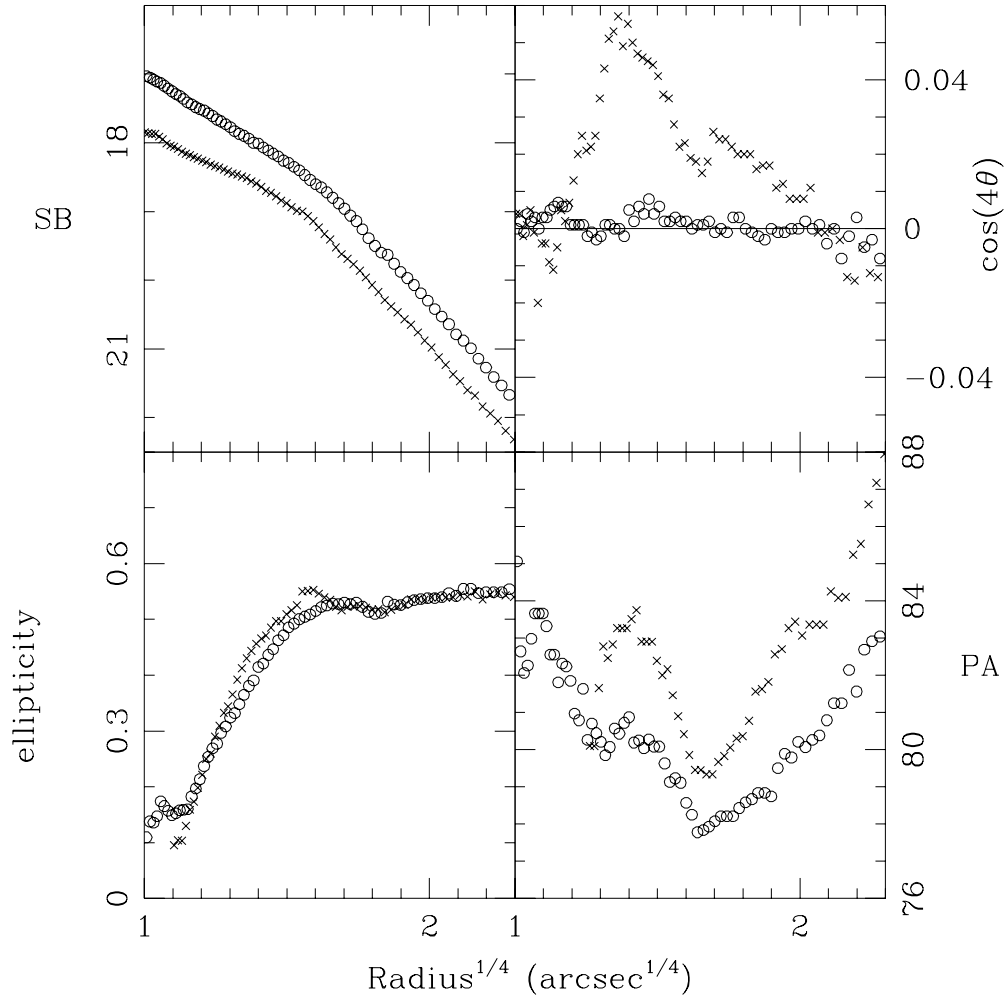


Fig. 4

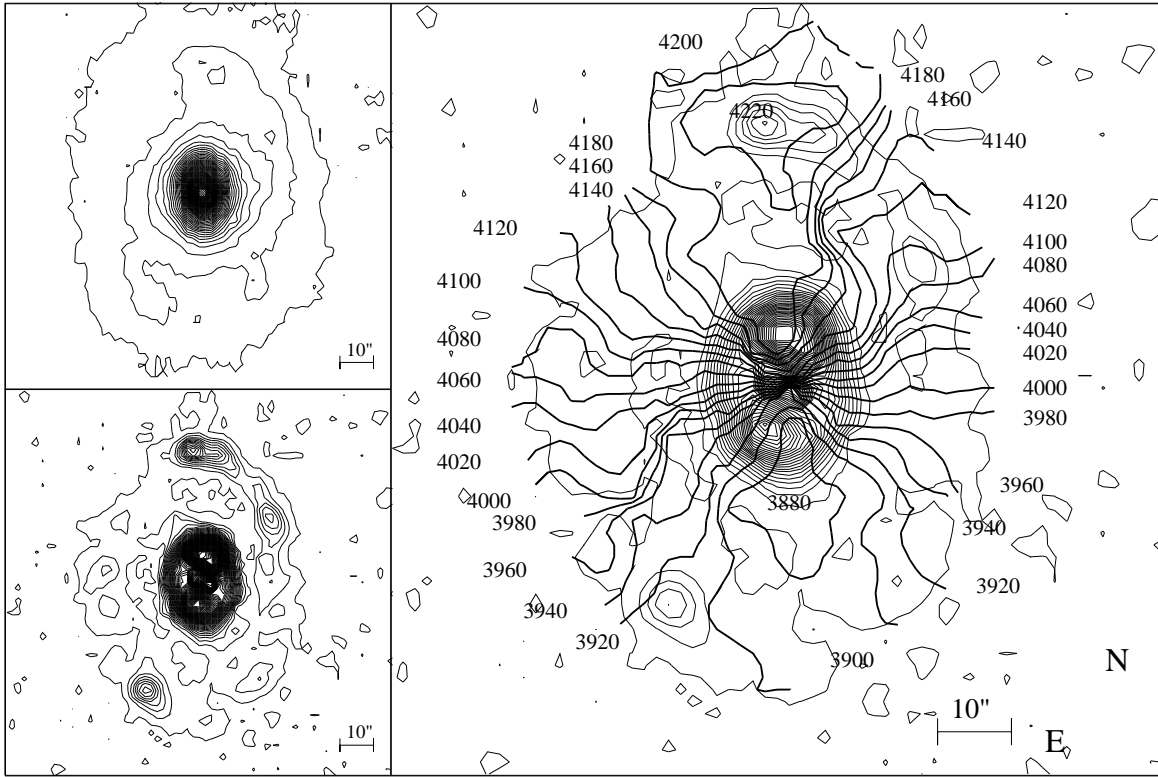


Fig. 5

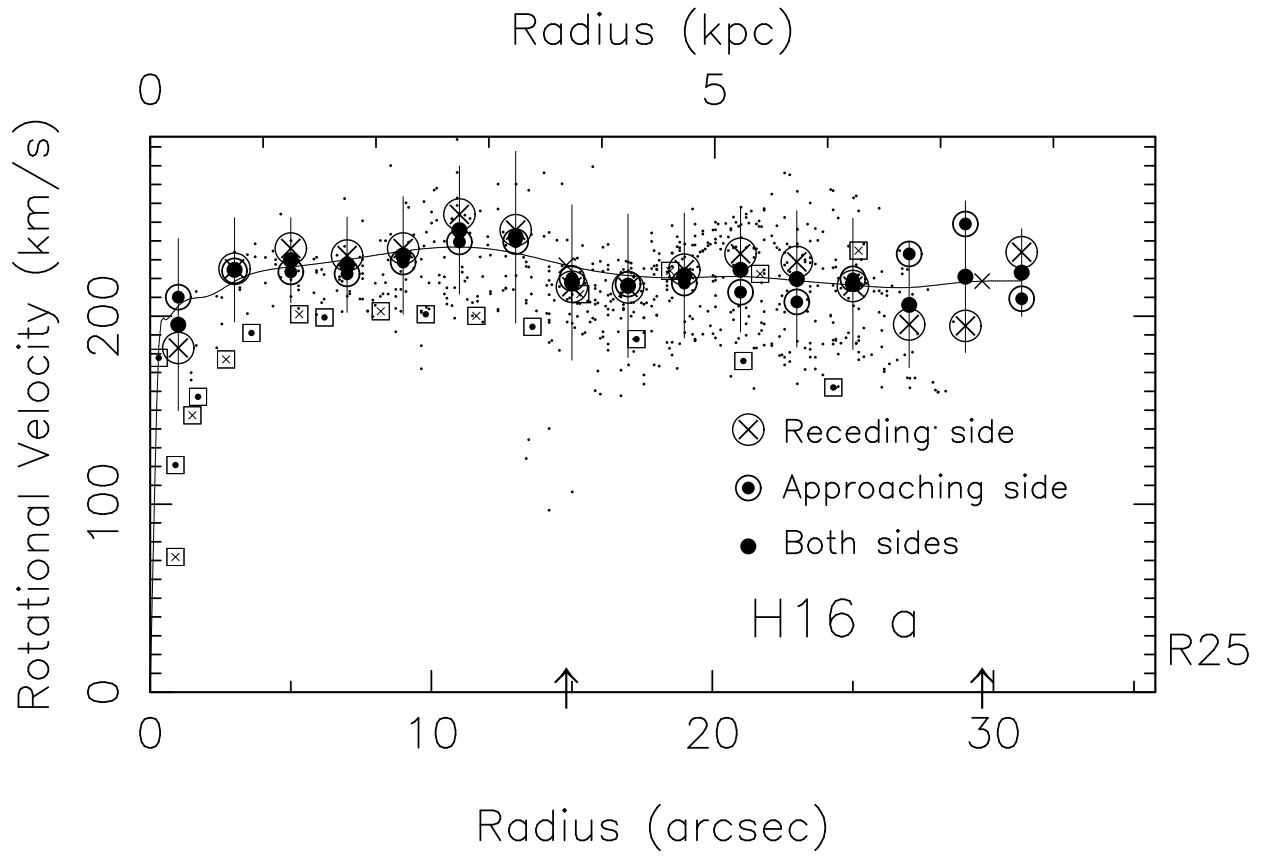


Fig. 6

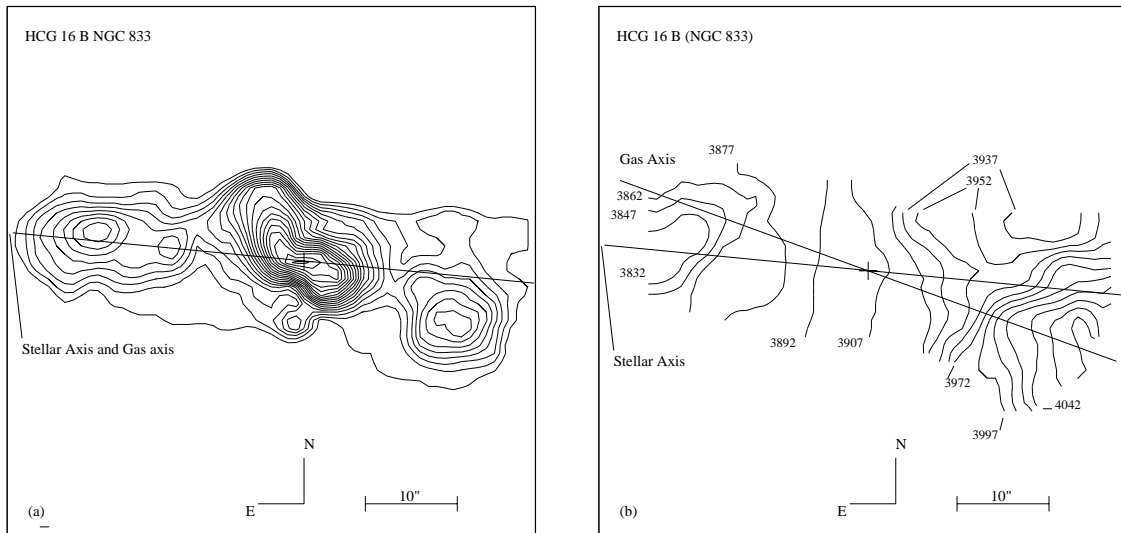


Fig. 7

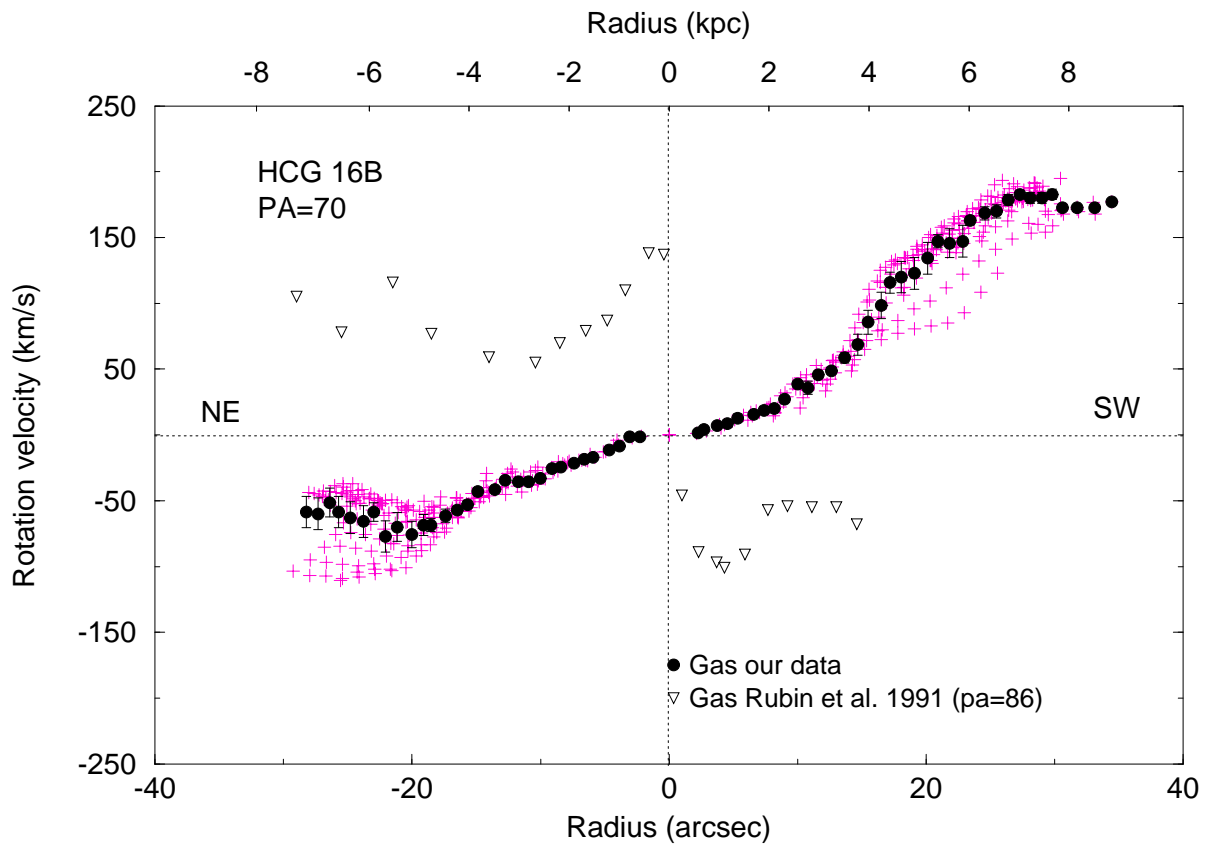


Fig. 8

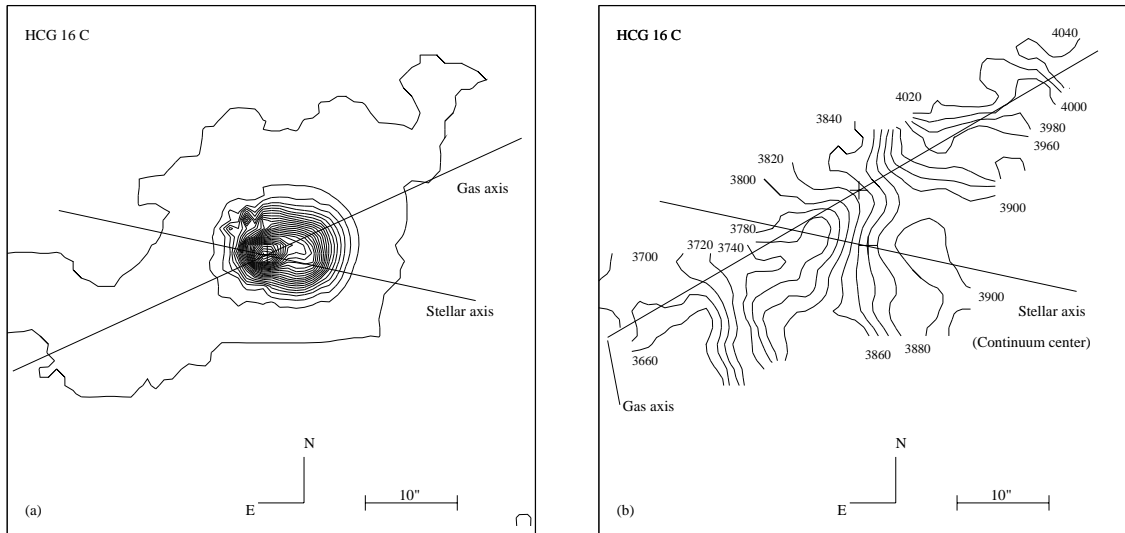


Fig. 9

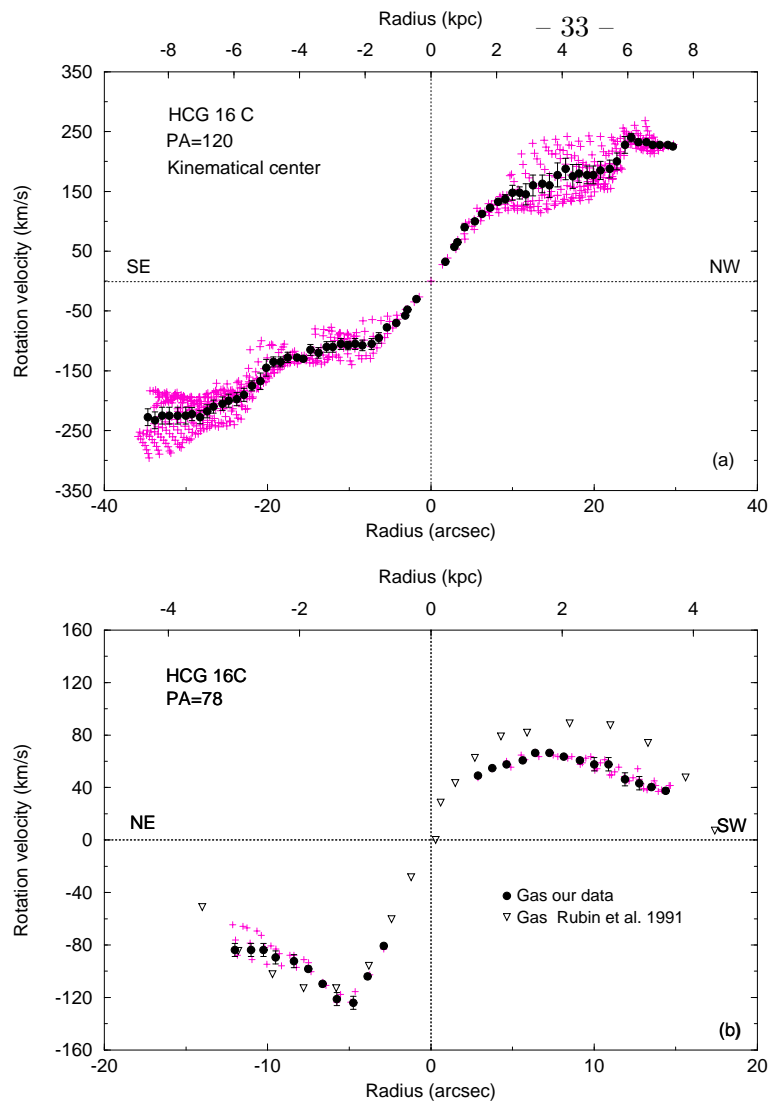


Fig. 10

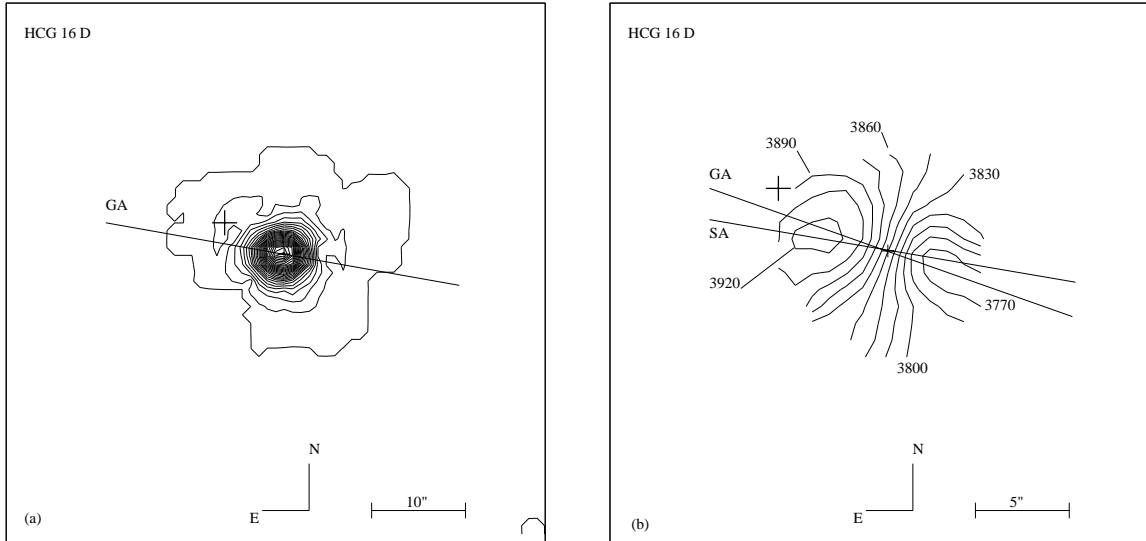


Fig. 11

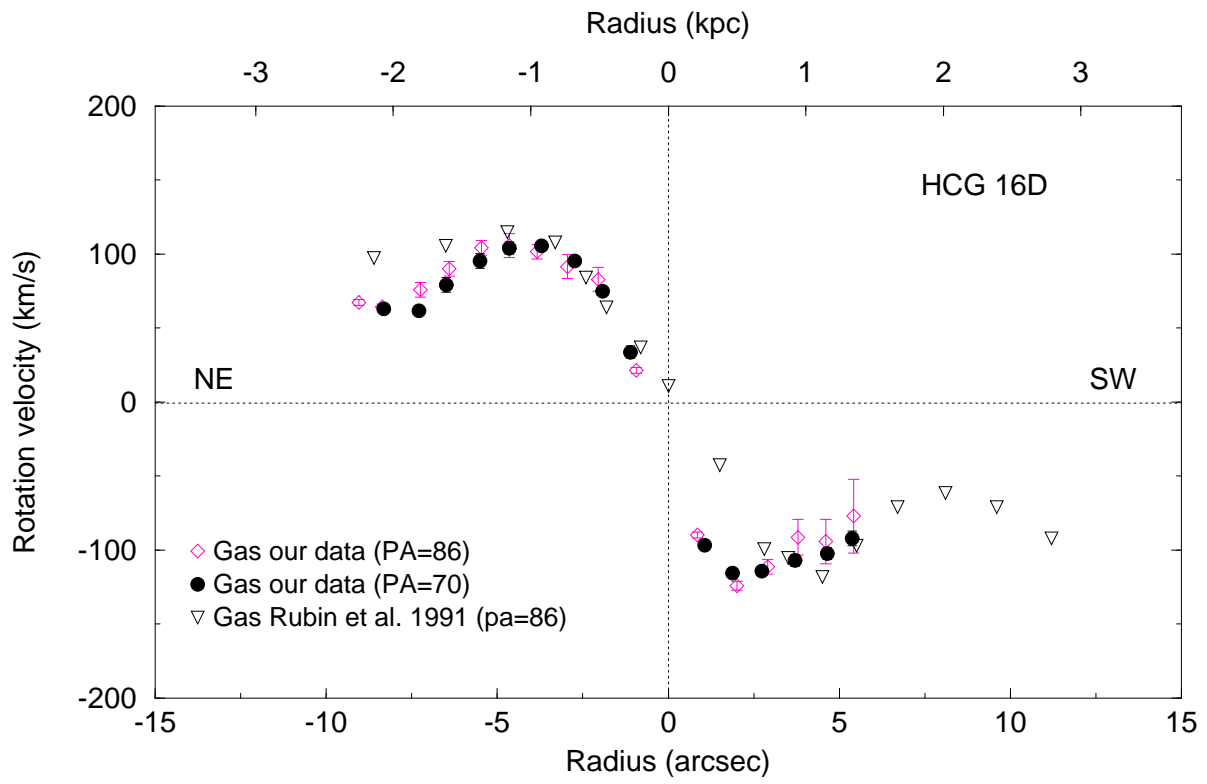


Fig. 12

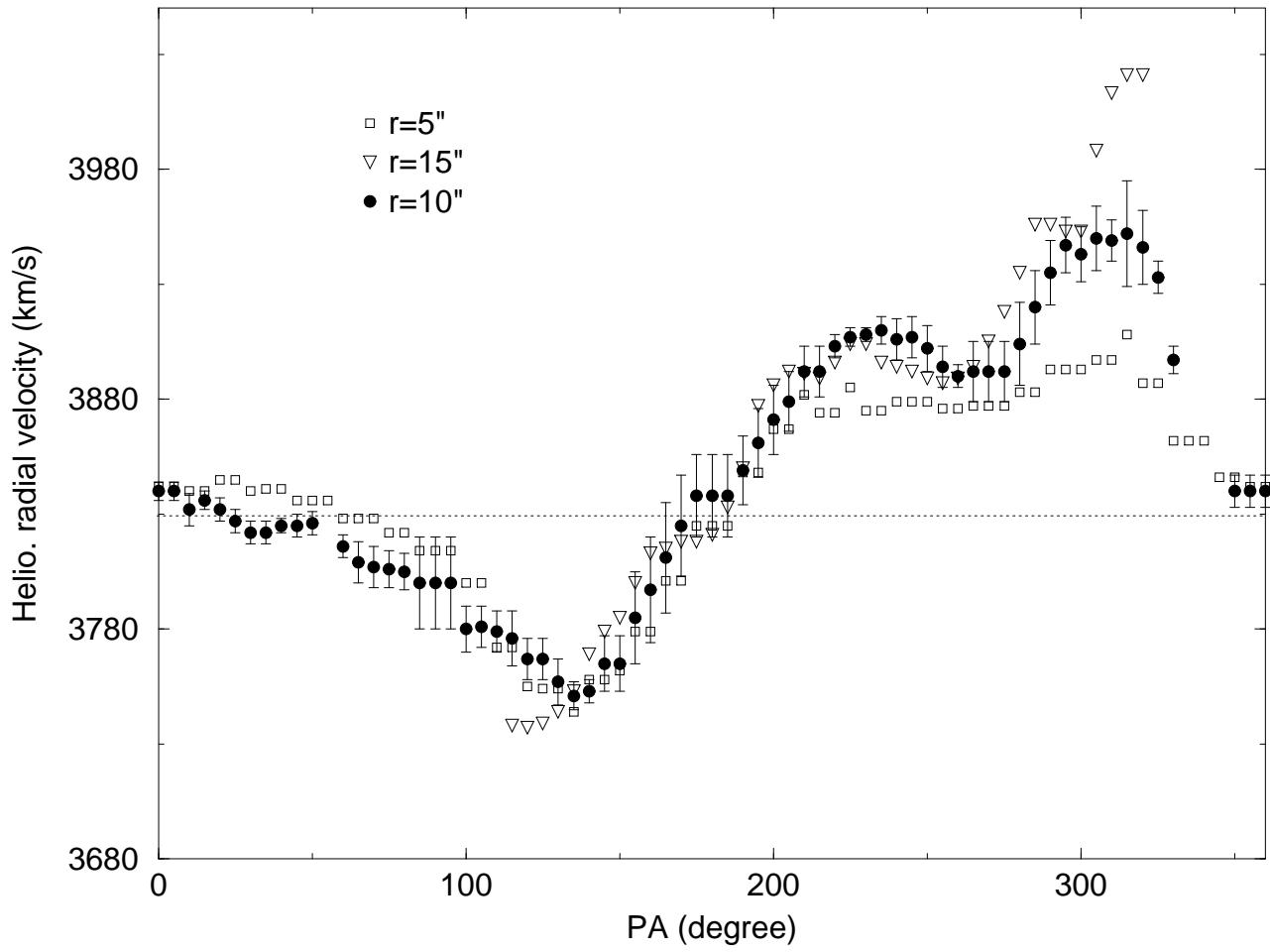


Fig. 13